J Mater Sci (2007) 42:5381–5390
DOI 10.1007/s10853-006-0886-x

The effect of porogen on physical properties in MTMS–BTMSE spin-on organosilicates

B. R. Kim · J. M. Son · M. J. Ko

Received: 1 June 2006 / Accepted: 24 August 2006 / Published online: 23 March 2007
© Springer Science+Business Media, LLC 2007

Abstract Decreasing the circuit dimensions is driving the need for low-k materials with a lower dielectric constant to reduce RC delay, crosstalk, and power consumption. In case of spin-on organosilicate low-k films, the incorporation of a porogen is regarded as the only foreseeable route to decrease dielectric constant of 2.2 or below by changing a packing density. In this study, methyltrimethoxysilane (MTMS)–bis(trimethoxysilyl)ethane (BTMSE) copolymers that had superior mechanical properties than MSSQ (methyl-silsesquioxane) were blended with amphiphilic block copolymers used as sacrificial pore generators. While adding up to 40 wt.% porogen into MTMS:BTMSE = 100:50 matrix, optical, electrical, and mechanical properties were measured and the pore structure was also characterized by positron annihilation lifetime spectroscopy (PALS). The result confirmed that there existed a tradeoff in attaining the low dielectric constant and desirable mechanical strength, and no more pores than necessary to achieve the dielectric objective should be incorporated. When the dielectric constant was fixed to approximately 2.3 by controlling BTMSE and porogen contents simultaneously, the thermo-mechanical properties of the porous films were also investigated for the comparison purpose. Under the same dielectric constant, the concurrent increase in BTMSE and porogen contents led to improvement in modulus measured by the nanoindentation technique but deterioration of adhesion strength obtained by the modified edge lift-off test.

B. R. Kim (✉) · J. M. Son · M. J. Ko
LG Chem. Ltd., Research Park, 104-1 Moonji-dong, Yuseong-gu, Daejeon 305-380, Korea
e-mail: brkim@lgchem.com

Introduction

Interconnects between transistors are composed of thin metal wires and the dielectric films which isolate them from each other to prevent shorts. Traditionally, interconnect materials are aluminum as a metal line and silicon dioxide as an insulating layer. However, the continuing evolution of microelectronic device requires new interconnect materials that can accommodate the miniaturization. Copper having lower electrical resistance and better electromigration resistance than aluminum has proved to be a feasible solution as an alternate metal, but no new dielectric material has emerged as a clear winner since the properties that low dielectric constant (low-k) materials require are so diverse and stringent. According to ITRS roadmap, the dielectric constant suitable for 152 nm pitch is 2.4 by the year 2007, and the value demanded for 54 nm pitch should be smaller than 2.0 by the year 2016 [1].

In order to develop new low-k materials with the dielectric constant lower than 2.4, two general approaches are mainly adopted. The first option is a homogeneous alternative to incorporate atoms and bonds with lower polarizability. Incorporation of fluorine atoms is particularly effective in reducing the dielectric constant since the high electronegativity of the atoms leads to tight binding of electrons [2, 3]. Moreover, fluorine atoms have a role in increasing the interatomic distance, which offers an additional decrease of the dielectric constant. Introducing porosity into base matrix materials is the other preference to reduce the density. The porous films are generally synthesized using a sacrificial porogen approach by blending a thermally labile porogen with a thermally stable matrix resin [4]. The network of nanopores is embedded into a rigid dielectric matrix as a result of the polymerization of the resin precursors, the decomposition and the volatiliza-

tion of the porogen during thermal cure. The dielectric extendibility to materials with the lower dielectric constant is allowed by controlling the content of pores, or voids filled with air.

However, one of the fundamental dilemmas for developing low-k dielectrics is the fact that a low dielectric constant is incompatible with high mechanical stability, particularly for porous materials whose mechanical properties are generally deteriorated further by a presence of pores. Although it is not clear which mechanical property is the most important one for successful integration, it is evident that decent mechanical strength should be ensured to survive the harsh semiconductor fabrication processes. This observation supports that no more porosity than necessary to achieve the dielectric objective should be incorporated. Not only the volume fraction of the pores but also pore size, shape and distribution are the critical factors that affect the physical properties of porous low-k films. The increase in porosity is inclined to enlarge the pore size and makes the pores become percolated and interconnected when porosity exceeds about 20–30%. Since the percolated channel in the material gives rise to reliability concern such as moisture absorption, metal diffusion, and crack formation, the porous low-k films with homogeneous and nanometer-sized closed pores are preferred to preserve physical properties.

Considerable studies have been done on spin-on porous low-k films to investigate the impact of the porogen loading on physical properties. In many cases, methyl-silsesquioxane (MSSQ) was used as a base matrix material and has been modified by blending various organic pore-generating polymers [5–8]. Though careful control in the preparation of porous films offered flexibility of the physical properties, the introduction of pores inevitably deteriorated mechanical properties. Accordingly, the modulus of porous MSSQ film with dielectric constant of 2.3 did not exceed 4 GPa at the very most due to the low modulus of unmodified MSSQ films. Introducing hydrogen-silsesquioxane (HSSQ) as a base material did not make the situation much different, which explained that the development of suitable matrix materials with superior physical properties kept up with the finding of properly designed sacrificial polymers [9, 10]. Toivola et al. lately measured the physical properties of porous methyltrimethoxysilane (MTMS)–bis(trimethoxysilyl)ethane (BTMSE) copolymer film and concluded that the copolymer films (MTMS:BTMSE = 9:1 mol%) had better mechanical properties than MSSQ films since the addition of BTMSE with greater functionality than MTMS enhanced network formation [11]. Considering that the improvement of mechanical properties was not eternally proportional to the amount of BTMSE, MTMS–BTMSE copolymers with five different compositions were synthesized and their physical properties were characterized to find optimum amount of BTMSE [12].

In the present study, five different MTMS–BTMSE copolymers were blended with up to 40 wt.% porogen to systematically investigate the influence of porogen content on pore structure and physical properties. The pore structure was characterized by positron annihilation lifetime spectroscopy (PALS) using radioactive β-decay positrons. The variations of optical, electrical, and mechanical properties of the copolymers were also investigated. In addition, the porous films having the same dielectric constant of 2.3 were synthesized by controlling porogen content in accord with the variation of BTMSE content in the matrix resin, and their mechanical properties were recorded for comparison purpose.

Experimental

Material synthesis and film processing

The porous organosilicate films were prepared by the following procedures. First, MTMS–BTMSE prepolymers were mixed with deionized water and solvent with stirring. 0.5–5.0 equivalent of deionized water per each alkoxy group was added, and the concentration of reaction mixture was adjusted to 1–3 M by water and solvent. Second, deionized water including a catalytic amount of HNO_3 was blended to this solution at the room temperature and stirred for 30 min or longer. Acid catalyst was added in molar ratio of 5×10^{-3} to 5×10^{-2} relative to the mol of silicate precursor. Under these conditions, the turbid solution turned clear after a few minutes. This mixture was stirred at 50–80°C over 6 h (generally 6–30 h) and then cooled to the room temperature. To this mixture was added high boiling point solvents mentioned above. Low boiling point components were removed from the resulting reaction mixture through the vacuum evaporation method at 45 °C, which led to the final matrix solution containing the prepolymers with average molecular weights of 1,000–3,000. To the matrix solution, the commercially available triblock copolymer, T1301, was loaded from 0 to 40 wt.% to produce porosity during subsequent curing step.

The coating solution was applied to a 101.6 mm (4 in.) silicon wafer with a spin coater at the acceleration rate of 1,000 rpm/s and the spinning rate of 2,000 rpm/s for 30 s. The deposited films were uniform, defect-free, and reproducible after several repetitions of experiments. After deposition, the films on wafer were dried for 2 min on a hot plate maintained at the temperature of 100 °C to thereby remove the solvent. Subsequent annealing was usually performed for 60 min at 430 °C under N_2 environment, which was attributed to form a colorless transparent porous films. The thickness of the films ranged from less than 0.1 μm up to 2.0 μm, depending on the spin speed and the

solid content of coating solution. Unless indicated otherwise, all experiments were performed after 430 °C annealing. A schematic diagram used to produce porous low-k films is summarized in Fig. 1.

Characterization

Thermal stability with regard to decomposition of the porogen was determined using thermogravimetric analysis (TGA 2950, TA instrument), which measured weight loss as a function of temperature. Temperature was ramped up to 430 °C with 3 °C/min heating rate under N_2 environment. Final solid contents of coating solutions were fixed to 20 wt.% in proper coating solvents.

Refractive index and thickness of porous films were extracted by ellipsometry (Jobin Yvon UVISEL™) that was a very sensitive and nondestructive method suited for investigating transparent films [13]. Both the parameters were extracted by curve-fitted ellipsometric values (Ψ and Δ) that were measured with 70° fixed angle of incidence and at 632.8 nm wavelength. The ellipsometric values were attained by measuring the nine different points of a single film and then averaging these. The deviation of these nine points was less than 0.3%, which supported the reliability of dielectric constant results that demanded accurate

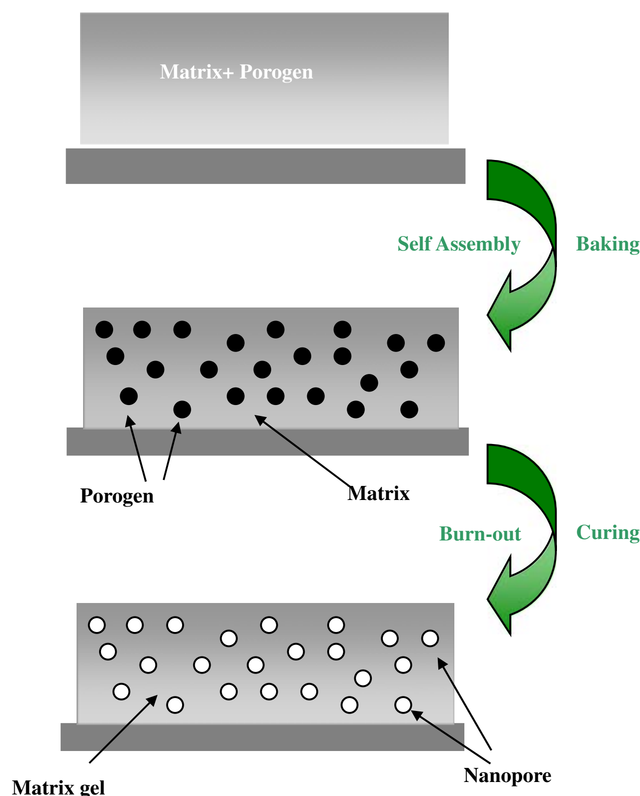

Fig. 1 Schematic flowchart to produce porous low-k films

thickness values on their calculation. Dielectric constants of the porous films were measured with metal–insulator–semiconductor (MIS) structures at room temperature in air. After aluminum electrodes of 2 mm and thickness of 120 nm were deposited on low-k films with an electron beam evaporator, electrical capacitance on eight dots was measured while DC voltage was swept from –40 V to 40 V at a frequency of 1 MHz. The dielectric constant was calculated from the known relationship between thickness and the capacitance averaged over eight dots.

Both elastic modulus and hardness were achieved using the continuous stiffness measurement technique on a MTS nanoindenter XP equipped with the DCM head [14]. In this technique, an extremely small sinusoidal oscillation was superimposed on the load ramp and the dynamic response of the contact was determined, which allowed the hardness and modulus of the material to be extracted continuously throughout the indentation process. The system had a displacement and load resolution of 0.0002 nm and 50 nN. Prior to testing each film, the calibration of the instrument and the determination of area function were performed by indenting fused silica with a modulus of 72 GPa. Due to an elastic isotropy and low modulus to hardness ratio, the sample has been normally employed for standard calibration material. It was indented to a load of up to 10 mN with Berkovich (three-side pyramid shape) indenter. Based on the calibration result, the test on each sample was carried out up to 200 nm depth at a frequency of 75 Hz by using the same indenter, and the results were averaged over nine indents.

Residual stress was evaluated by Tencor FLX-2320 system that employed a laser scanning technique to sense deformation caused by thin films on a wafer [15]. Since every wafer had some initial curvatures and surface irregularities, measures were taken before and after films deposition. When the biaxial modulus of the substrate and thickness of the film and substrate was known in prior, the change in curvatures of the wafer could be converted into residual stress of thin films employing Stoney's equation.

The modified edge lift-off test (MELT) method was adopted to determine and compare fracture strength of low-k materials [16]. After epoxy backing layer with sufficient thickness was applied onto low-k films, the films were debonded from the substrates by lowering the temperature until the stored energy in the epoxy layer exceeded the adhesion energy at the specific interface. The temperature of delamination was detected by comparing a series of pictures taken by a digital camera and converted to residual stress by the predetermined stress versus temperature relation. For each copolymer sample, 18 small coupons with the size of 13 × 13 mm^2 were tested and the results were averaged to calculate interfacial fracture toughness Table 1.

The micropore and mesopore sizes as well as pore interconnectivity were measured by PALS at room temperature [17, 18]. In using PALS with thin films, an electrostatically focused beam of several keV positrons generated in a high vacuum system was implanted into the samples. The uncapped samples were investigated at several implantation energies, 2.0, 3.0, and 5.0 keV, to search for any depth-related heterogeneity. In case of the thin film with open pores, 60 nm silicate cap was deposited to confine positronium (Ps), the bound state of a positron and electron, to the pores in the film, which allowed the measurement of the intrinsic pore size in an interconnected porous network. Ps was formed by electron capture and traps in the void volume of pores, and then pore size could be calculated with its annihilation lifetime (2–142 ns) with extended Tao-Eldrup model [19].

Results and discussions

T1301 used as a porogen was an amphiphilic polymeric surfactant and a good candidate material for template because it could microphase separate into nanometer-scale domains. TGA data indicated that decomposition of the porogen polymer occurred between 270 °C and 400 °C, and approximately 1.0 wt.% of residue remained after 430 °C heating.

The previous study for MTMS–BTMSE copolymer matrix showed that the more amounts of BTMSE added, the further condensation reaction was promoted, which led to the higher crosslinking density [12]. As a result, most of the physical properties became proportional to the amount of BTMSE though their increasing rates were different. The current study focused on the influence of porogen contents on physical properties by loading different amounts of porogen into five MTMS–BTMSE copolymers. While the monomer content of BTMSE varied from 9.1 to 47.3 mol% versus MTMS, porogen loading weight fraction loaded for each copolymer ranged from 0 to 40 wt.%.

Figure 2a plots the refractive index measured by ellipsometer as a function of porogen loading. The refractive index decreased monotonically over the entire compositional range with the increase in porogen loading, which implied that the pores were efficiently generated without pore collapse or film shrinkage upon the thermal cure. Figure 2b shows volume fraction porosity extracted from Lorentz–Lorentz equation:

$$\frac{n_0^2-1}{n_0^2+2}\times(1-P)=\frac{n^2-1}{n^2+2} \quad (1)$$

where n_0 and n represent refractive indices of base matrix material and porous film, and P denotes volume fraction porosity. The difference between the volume fraction porosity and weight percent porogen loading was due to the fact that the matrix resin itself lost some of its initial weight upon curing. Porogen loading, which was calculated on a weight percent basis, also contributed to the difference. In addition, the presence of micropores was another reason of the inconsistency. The previous works showed that MSSQ film prepared with 1% of porogen already contained 14–16 vol.% micropores [20]. The works also proved that porogen concentration was not correlated with full porosity, but it was equal to mesopore volume. It was conjectured that such a large amounts of micropores were formed by the steric hindrance effect of alkyl groups. As shown later, PALS analysis of the current porous MTMS–BTMSE films also confirmed the presence of micropores in base materials though the analysis cannot specify the amounts quantitatively.

Figure 3 represents the dielectric constant calculated from the capacitance that was measured with MIS structures. Scattering of its measured value was due to the characteristics of the dielectric constant sensitive to environmental effects such as humidity and metal contamination. The scattering became severer with increasing porogen since the film with higher porosity reacted more sensitively to the environmental effect. This observation was based on the fact that the dielectric constant of MTMS:BTMSE = 100:50 at 40% porogen loading was measured higher than that of MTMS:BTMSE = 100:90 at the same porogen loading. It has been known that the

Table 1 Physical properties of porous organosilicates with different porogen content in MTMS:BTMSE = 100:50 copolymer

Porogen content (%)	0%	10%	20%	30%	40%
Refractive index	1.437	1.368	1.315	1.264	1.214
Thickness (nm)	890	860	850	860	860
Dielectric constant	2.92 ± 0.01	2.71 ± 0.02	2.39 ± 0.01	2.15 ± 0.01	1.92 ± 0.02
Reduced modulus (GPa)	11.85 ± 0.22	7.80 ± 0.14	4.73 ± 0.07	2.99 ± 0.07	1.86 ± 0.05
Hardness (GPa)	1.77 ± 0.04	1.09 ± 0.03	0.61 ± 0.01	0.37 ± 0.01	0.22 ± 0.01
Residual stress (MPa)	92.3 ± 1.3	75.4 ± 1.0	50.2 ± 0.8	36.0 ± 0.4	32.7 ± 0.5
Fracture toughness (MPa $m^{0.5}$)	0.202 ± 0.003	0.190 ± 0.002	0.179 ± 0.003	0.174 ± 0.004	0.170 ± 0.006

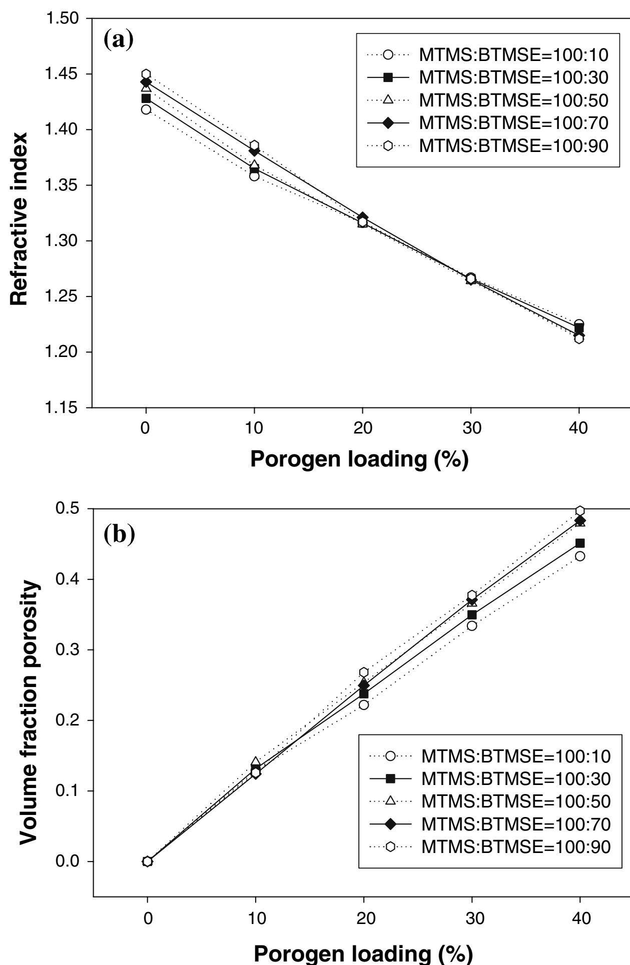

Fig. 2 (**a**) Refractive index of porous MTMS–BTMSE copolymers as a function of porogen loading, (**b**) volume fraction porosity of MTMS–BTMSE copolymers calculated by using Lorentz–Lorentz equation

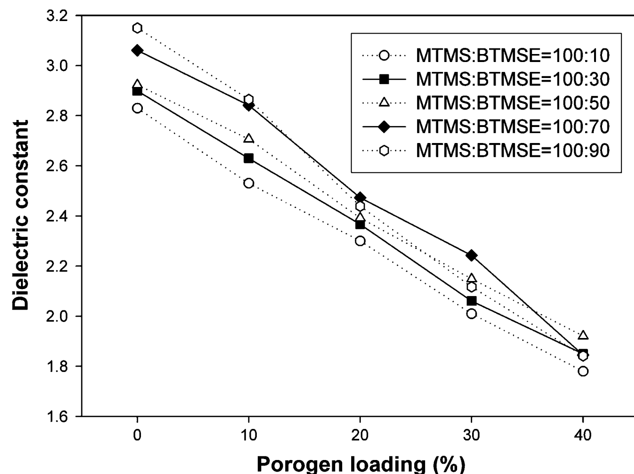

Fig. 3 The dielectric constant of porous MTMS–BTMSE copolymer films as a function of porogen loading

refractive index and the dielectric constant at a frequency of 1 MHz provided the information of the electronic and nuclear components of the dielectric constant. While the electronic component was associated with the refractive index or bond density, the nuclear component was dominated by the polar substituents or defect functionals remained in the films. As the amount of porogen loading increased, the absolute number of functional endgroups capable of inducing condensation reaction seemed to be on the decrease, and then less unreacted functionals remained in the films after cure. As a result, the percentage of the electronic component became superior to that of the nuclear component with increasing porogen loading though the dielectric constant for porous film was mainly related to the refractive index.

Figure 4a represents nanoindentation test results for MTMS:BTMSE = 100:50 copolymer films as a function of indented depth. For current low-k films whose normal thickness was less than 1 μm, the indented depth was limited up to 200 nm. Each sample in this test was indented nine times for averaging. The load–depth curve illustrated that the indented depth was so small that elastic contact was dominant as well as the mode of plastic deformation could hardly occur. AFM images scanned on the indentation site also supported this observation. Even though the sample was indented by the sharp Berkovich tip, no permanent deformation was found up to 200 nm indentation depth. From the load versus indented depth profiles, reduced modulus and hardness could be calculated without difficulty. Figure 4b demonstrates reduced modulus as a function of normalized indentation depth defined as indentation depth divided by film thickness. The preliminary test results indicated that modulus profiles of films with different thickness were coincident with each other within the test range when the indented depth was normalized to film thickness. As expected, modulus decreased with the increase in porogen loading, which was mainly due to the decrease in the film density. In addition, as the amount of porogen loading increased, the substrate effect started to appear at higher indentation depth. Modulus at 40 wt.% porogen in this situation kept almost constant until the indented depth approached 20% of film thickness. Figure 4c shows hardness versus normalized indentation depth curve. While hardness could be correlated with yield strength when enough indentation depth was guaranteed, it was difficult to induce information about plastic properties for very thin films since the indented depth was limited and then elastic contact was dominant. The comparison between Fig. 4b and c merely suggested that the variation of the hardness was much slower than that of modulus since the former was less sensitive to the substrate effect than the latter. In general, the minimum values observed in the modulus and hardness profiles were regarded as the gen-

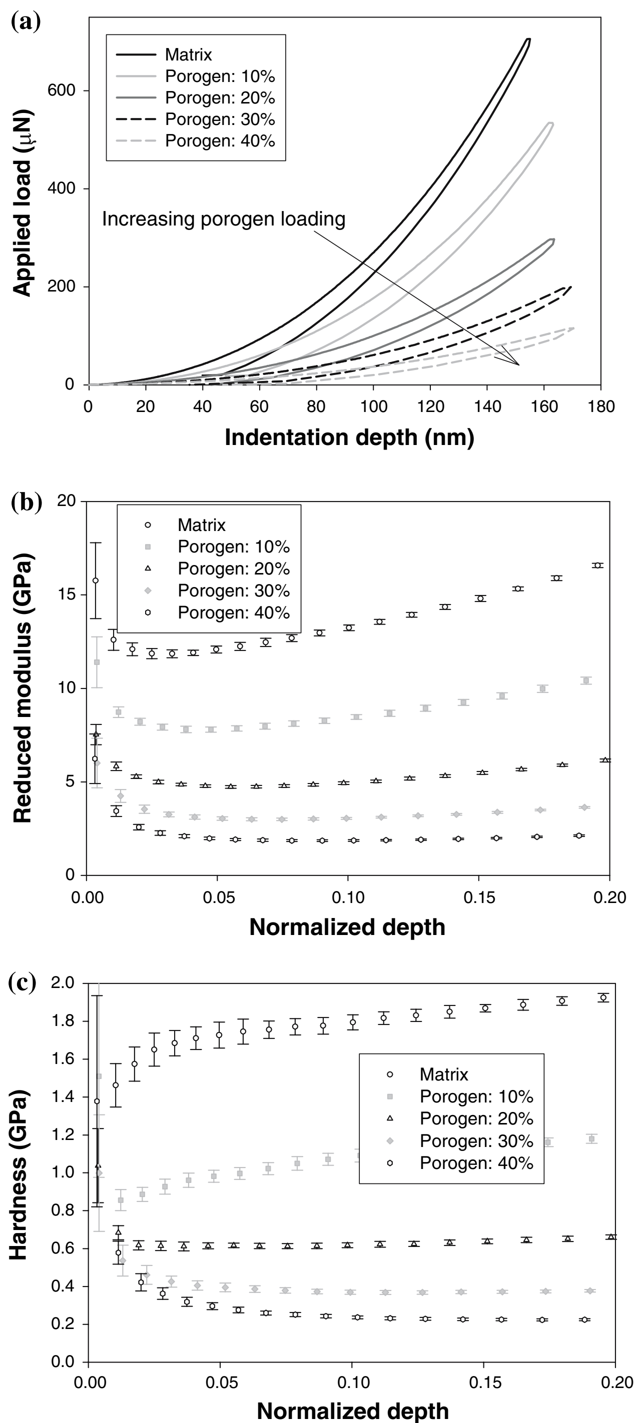

Fig. 4 (**a**) Load versus indentation depth profile, (**b**) reduced modulus, and (**c**) hardness as a function of normalized indented depth for porous MTMS:BTMSE = 100:50 copolymer films

uine properties of the low-k films in the microelectronic society. According to this conventional definition, hardness became proportional to modulus in spite of certain differences in the trend of both profiles since both values were read in elastic contact region.

Figure 5a describes the modulus as a function of porogen loading. The dramatic decrease in modulus with increased porogen loading implied that the relationship between the two was not linear, but the decrease showed a power law variation with exponent. Earlier, Gibson and ashby described the relationship between modulus and porosity for open-cell foam with the following equation [21].

$$E_f/E_m = (1 - P)^n \tag{2}$$

where E_f is the modulus of porous film, E_m is the modulus of nonporous film, and P represents porosity. The exponent, n, is 2 for foams with open pores and is generally less than 2 for the case of closed-cell foam. Though higher order information such as the ratio of pore wall thickness to diameter, the pore connectivity, and pore wall non-uniformity as well as the porosity enabled more accurate

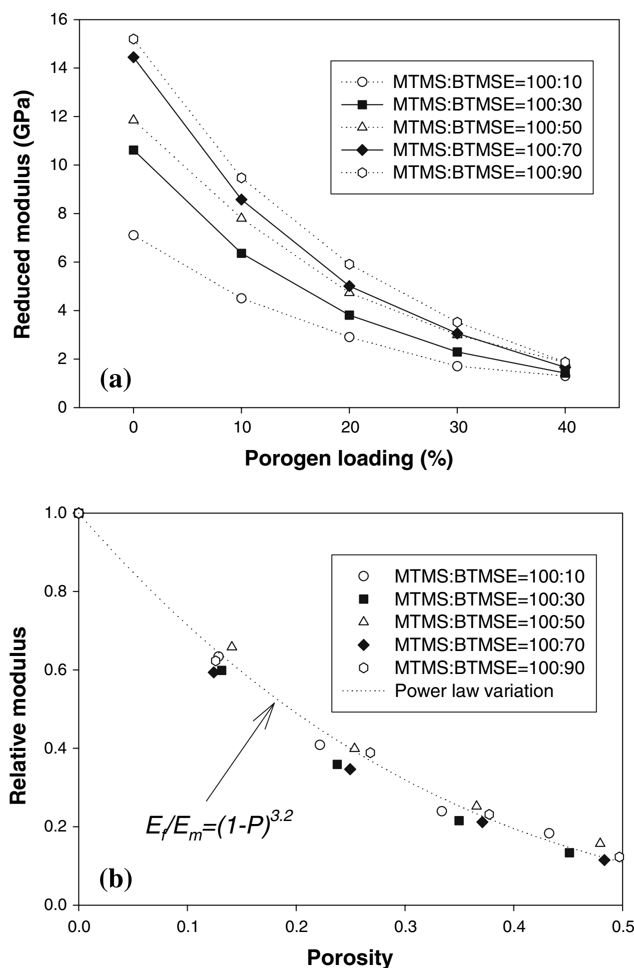

Fig. 5 (**a**) Reduced moduli as a function of porogen loading and (**b**) relative moduli of porous MTMS–BTMSE films as a function of porosity calculated by Lorentz–Lorentz equation

expression, the power law expression has been widely accepted due to its simplicity [22].

In order to investigate how the exponent varied with the kind of matrix materials, modulus of each porous film was normalized with that of matrix film, which was shown in Fig. 5b. Instead of porogen loading, porosity extracted from Lorentz–Lorentz equation was used in the horizontal axis. Surprisingly, the normalized moduli were coincident with each other regardless of the composition of matrix materials. The modulus deteriorated much faster for less porosity so that it reached approximately 70% of initial value at the porosity of 0.1. A fitted exponent in the Eq. 2 was found to be 3.2, which was a much higher value than expected. Several studies already reported the same trend [14, 23–25]. Such a high exponent explained that increasing porosity not only increased pore volume but also contributed to decreasing the matrix networking. However, it is still questionable whether the same exponent can be applied to similar copolymer films, and it remains as an issue to be discussed further in detail.

Not only modulus and hardness that have been mostly employed to evaluate the mechanical strength of the low-k films, the residual stress was also one of the important properties that could impact the device reliability and lifetime. The stress was originated by the shrinkage from the evaporation of the residual solvent as well as the stress of the film resulting from the difference in the coefficient of thermal expansion between the film and the substrate. Taking into account that each porous film was spin-coated on the same substrate, the magnitude of the stress mainly relied on the thermal expansion coefficient and elastic modulus of the film. It has been known that the thermal expansion coefficient stayed constant regardless of the porosity for open-cell foam, but it was a function of porosity for closed-cell foam due to the pressure of the gas kept inside the foam [21, 26]. Even for low-porosity materials composed of a closed-cell structure, however, the gas expansion inside the cells was not significant, and then the thermal expansion coefficient of the porous film was close to that of matrix materials. Therefore, it can be said that the magnitude of the residual stress was proportional to the modulus of the film.

Figure 6a illustrates the behavior of the residual stress as a function of porogen loading for MTMS:BTMSE = 100:50 copolymer matrix. The rate of decrease seemed to be almost linear for the porogen loading less than 30%, and the stress approached an asymptotic value of approximately 30 MPa at the porogen loading in excess of 40%. The steady decrease in the residual stress with the increase in porogen loading was already observed for porous MSSQ film [4]. Though the trend of current porous films was close to porous MSSQ films, the decrease rate was much slower than that of modulus measured by the nanoindentation method. This inconsistency was originated from the inhomogeneous and anisotropic nature of the films. Gostein and coworkers showed that in-plane modului of porous films were much higher than the out of plane modulus due to preferential orientation of the pores [27]. Vellery et al. also presented the inhomogeneous pore distribution of SiCOH film with depth profiled PALS analysis [28]. The surface layer composed of isolated pores was relatively dense, and the pores had slightly larger radius toward the bottom of the film. Considered that modulus and residual stress were calculated under the assumption of inhomogeneous and anisotropic film, it can be concluded that the deviation was not significant.

Figure 6b plots the change in fracture toughness as a function of porogen loading for the same porous films. As porogen loading increased, fracture toughness was monotonically deteriorated, and its standard deviation was inclined to increase. The MELT method was generally employed to evaluate the adhesion strength that could be measured when low-k films were completely removed from the silicon substrate. In some cases, however, low-k films were torn away piece by piece from the substrate, which

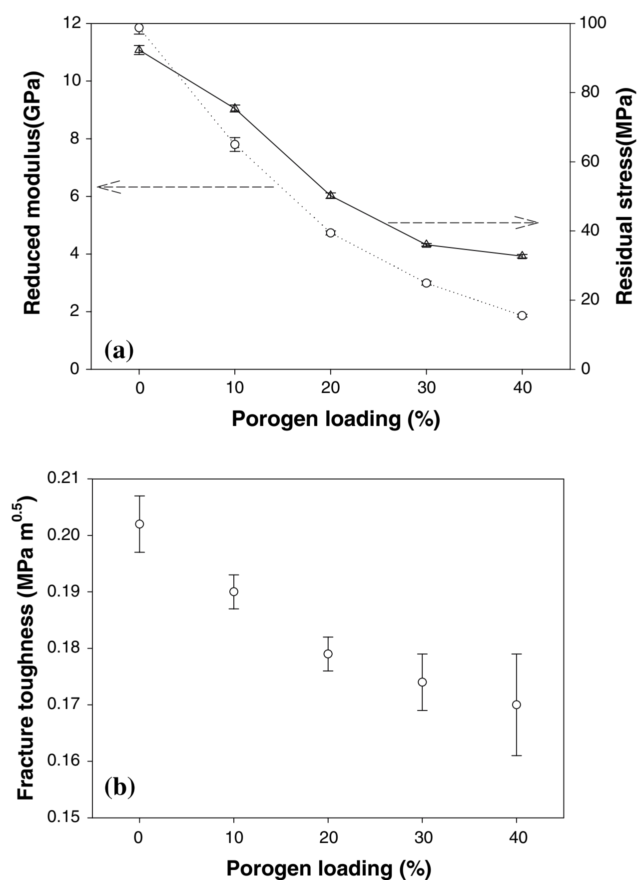

Fig. 6 (**a**) Residual stresses and reduced moduli as a function of porogen loading, (**b**) interfacial fracture toughness as a function of porogen loading for porous MTMS:BTMSE copolymers

could be ascertained to crack deflection and crack bridging mechanism governed by the presence of pores. In order to interpret if the failure was purely related to adhesive fracture, it might be necessary to investigate the failure locus for each sample. Regardless of whether the sample exhibited adhesive or cohesive fracture behavior, it was evident that fracture resistance of the porous films reduced with increasing porosity.

A detailed PALS study was also performed for the same copolymer films. Table 2 shows the mean pore diameter deduced from Ps lifetime by using either a spherical or cylindrical pore model for varying porogen loading. In addition, the pore mean free path (4*V*/*S*, where *V* and *S* are the pore volume and surface area, respectively) range was set from the two pore models. The mean free path in a long cylinder was equal to the cross-sectional diameter, whereas the mean free path in a sphere was 2/3 the sphere diameter. The interconnection length in the last column represents the effective depth from which Ps can diffuse through the porous network and escape into the vacuum. Two short Ps components of 2.5 and 6.0 ns shown in the matrix film were related to Ps annihilating in micropores. The 2.5 ns lifetime component was typical of free volume voids in, for example, glassy polymers, and it matched up a spherical diameter of about 0.6 nm. The 6.0 ns lifetime component related to spherical pore diameter of 1.0 nm, and the intensity was so much higher than 2.5 ns that it was the dominant micropore. These micropore diameters were so close to each other that there might be a distribution of micropore diameters over this nominal range.

Different from nonporous matrix films, three porous films had higher Ps lifetime due to the mesopores of the films. While the Ps lifetime component less than 7 ns corresponded to micropores as explained, the component in the 15–50 ns range proved the existence in mesopores of porous films. The porous films with varying porogen concentration showed some degrees of pore interconnectivity and they all had some detectable Ps escaping into the vacuum. Pore size was very small for the 10 wt.% porogen loading film, and the pore interconnection length was estimated to zero. As the porogen loading increased, the pore size gradually increased and so did the Ps formation

Table 2 Summary of PALS results for the mesopores of the porous MTMS:BTMSE = 100:50 film

Porogen loading (%)	Ps lifetime (ns)	$D_{cylinder}$ (nm)	D_{sphere} (nm)	Mean free path (nm)	Interconnection length (nm)
0	2.5–6.0	–	0.6–1.0	–	0(closed)
10	16	1.4	1.7	1.1–1.4	0(closed)
20	34	2.1	2.6	1.7–2.1	<30
30	58	3,2	4.2	2.8–3.2	>500

fraction. Increasing porogen loading also led to the increase of the interconnection length. While the porous film with 10 wt.% porogen possessed low enough porosity to have closed pores, the film with 20 wt.% porogen was almost closed with the interconnection length less than 30 nm. The film with 30 wt.% porogen had highly interconnected pores of the order of the film thickness and can hence be considered to have fully interconnected pores.

Though PALS was a useful tool to measure the pore size and pore interconnectivity, it had a difficulty in determining absolute porosity since the overall porosity was directly related to fraction of Ps annihilated in the mesopores. Figure 7 represents the Ps intensity as a function of porogen contents. While the total amount of Ps was constant at approximately 20% for all samples, the fraction of mesopore Ps increased with increasing porosity at the expense of the micropore Ps intensity. This behavior demonstrated that Ps annihilated in the micropores was diffusing into mesopores and depopulating the micropore components. While the micropores in the matrix still remained in the porous films, the Ps moved through them and was trapped in the mesopores, leaving few Ps to annihilate in the micropores.

Though the investigation up to now has focused on the effect of porogen loading on the identical base matrix material, the amount of porogen loading needed to satisfy the target dielectric constant was also influenced by matrix materials. The result suggested that the target dielectric constant of the porous low-k films could be tailored not only by the porogen loading but also by the amount of BTMSE. Table 3 represents the thermo-mechanical properties of the porous films when the dielectric constant was fixed to approximately 2.3 by controlling BTMSE and porogen contents simultaneously. As expected, the necessary amount of porogen loading to satisfy the dielectric objective increased with the addition of BTMSE between

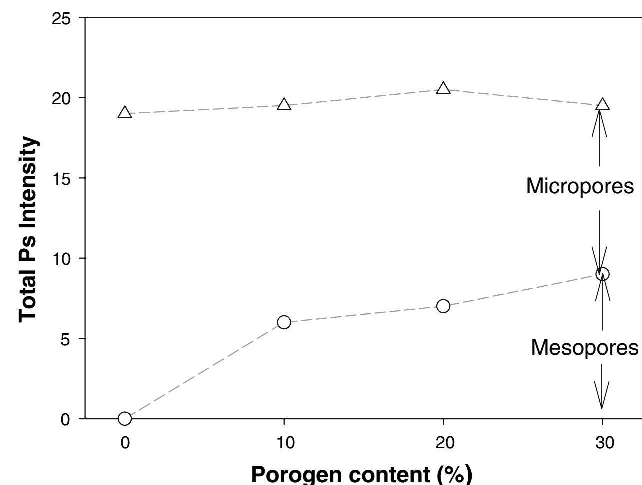

Fig. 7 The composition of the Ps intensity for MTMS :BTMSE = 100:50 film as a function of porogen contents

Table 3 Physical properties of porous low-k films with different BTMSE and porogen contents in MTMS–BTMSE copolymers

MTMS:BTMSE composition	100:10	100:30	100:50	100:70	100:90
Porogen content (%)	25	27	30	30	29.4
Dielectric constant	2.31 ± 0.01	2.35 ± 0.01	2.28 ± 0.01	2.27 ± 0.02	2.28 ± 0.01
Reduced modulus (GPa)	2.85 ± 0.01	4.27 ± 0.06	4.59 ± 0.08	5.33 ± 0.14	5.51 ± 0.14
Hardness (GPa)	0.37 ± 0.01	0.59 ± 0.01	0.63 ± 0.01	0.76 ± 0.04	0.72 ± 0.02
K_{IC} (MPa $m^{0.5}$)	0.186 ± 0.004	0.181 ± 0.005	0.174 ± 0.005	0.178 ± 0.003	0.162 ± 0.003

MTMS–BTMSE matrix copolymers. However, in spite of considerable differences in the BTMSE contents, the disparity in porogen loading was only less than 5%, which implied that increasing the amount of porogen loading was more effective than controlling BTMSE contents to lower the dielectric constant. For the porous films with the same dielectric constant, the modulus was inclined to increase with the increase in the amounts of BTMSE and porogen loading. Not specified here in detail, the decreasing rate of modulus with the increase in porogen content was almost identical over the specified compositional range for a series of porous MTMS–BTMSE polymers. The result suggested that the pores were efficiently generated for the copolymers and then modulus of each porous film could be predicted by measuring that of matrix unless pore collapse or film shrinkage happened.

Being different from modulus, fracture strength was gradually deteriorated with the increase in BTMSE and porogen loading. The previous study showed that interfacial fracture toughness of MTMS:BTMSE = 100:30 matrix (0.191 Mpa $m^{0.5}$) was much higher than that of MTMS:BTMSE = 100:10 matrix (0.166 Mpa $m^{0.5}$) [12]. However, the reversed fracture strength for both the porous films proved that the fracture toughness of porous films was highly dependent on the presence of pores rather than the strength of base matrix materials. The simultaneous increase in BTMSE and porogen contents had an advantage in improving modulus and hardness, but the increase deteriorated fracture strength. In addition, the increased possibility of generating interconnected pores with the increase in porosity might give rise to reliability concern.

Summary

Compared with MSSQ, MTMS–BTMSE copolymers blended with sacrificial porogen had superior mechanical properties. As the porosity increased, most mechanical properties except residual stress were deteriorated in return for attaining a low dielectric constant. Such a tradeoff in gaining the low dielectric constant and desirable mechanical strength implied that no more pores than necessary to achieve the dielectric objective should be incorporated. In addition to evaluating the physical properties, the pore structure and interconnectivity were characterized by PALS. PALS result for porous films with composition of MTMS:BTMSE = 100:50 indicated that the film with 20 wt.% porogen was almost closed but one with 30 wt.% porogen could be considered to have fully interconnected pores. This result suggested that it should be attempted to lower the porosity less than 20 wt.% to formulate the porous low-k films with homogeneous and nanometer-sized closed pores as well as to avoid the reliability concern caused by percolation. When the dielectric constant was fixed to approximately 2.3 by controlling BTMSE and porogen contents simultaneously, the thermo-mechanical properties of the porous films were also investigated for the comparison purpose. Under the same dielectric constant, the increase in BTMSE and porogen contents led to the improvement in modulus but the deterioration of adhesion strength. A lower-k starting material had an advantage in minimizing the amount of porosity but resulted in lower modulus to achieve target dielectric constant.

References

1. International technology roadmap for semiconductors. Semiconductor Industry Association, San Jose, CA (2003)
2. Hougham G, Tesoro G, Viehbeck A, Chapple-Sokol JD (1994) Macromolecules 27:5964
3. Lee S, Park J-W (1996) J Appl Phys 80:5260
4. Ho S, Leu J, Morgan M, Kiene M, Zhao J-H, Hu C (2003) In: Murarka SP, Eizenberg M, Shina AK (eds) Interlayer dielectrics for semiconductor technologies. Elsevier Academic Press, London, p 167
5. Miller RD, Beyers R, Carter KR, Cook RF, Harbison M, Hawker CJ, Hedrick JL, Lee VY, Liniger E, Nguyen C, Remenar J, Sherwood M, Trollsas M, Volksen W, Yoon DY (1999) Res Mater Soc Symp Proc 565:3
6. Huang QR, Volksen W, Huang E, Toney M, Frank CW, Miller RD (2002) Chem Mater 14:3676
7. Yang S, Mirau PA, Pai C-S, Nalamasu O, Reichmanis E, Pai JC, Obeng YS, Seputro J, Lin EK, Lee H-J, Sun J, Gidley DW (2002) Chem Mater 14:369
8. Padovani AM, Riester L, Rhodes L, Allen SAB, Kohl PA (2002) J Electrochem Soc 149:F171
9. Toivola Y, Thurn J, Cook RF (2002) J Electrochem Soc 149:F9
10. Liu W-C, Yu Y-Y, Chen W-C (2003) Mater Res Mater Soc Symp Proc 766:E7.10

11. Toivola Y, Kim S, Cook RF, Char K, Lee J-K, Yoon DY, Rhee H-W, Kim SY, Jin MY (2004) J Electrochem Soc 151:F45
12. Kim BR, Kang JW, Lee KY, Son JM, Ko MJ (2007) Physical properties of low-k films based on the co-condensation of methyltrimethoxysilane with a bridged silsesquioxane. J Mater Sci. DOI 10.1007/s10853-006-0575-9
13. Tompkins HG (1993) A user's guide to ellipsometry. Academic Press, Boston
14. Oliver WC, Pharr GM (1992) J Mater Res 7:1564
15. Zhao J-H, Malik I, Ryan T, Ogawa ET, Ho PS, Shih W-Y, McKerrow AJ, Taylor KJ (1999) Appl Phys Lett 74:944
16. Shaffer II EO, McGarry FJ, Hoang L (1996) Polym Eng Sci 36:2375
17. Gidley DW, Frieze WE, Dull TL, Sun J, Yee AF, Nguyen CV, Yoon DY (2000) Appl Phys Lett 76:128
18. Sun JN, Hu YF, Freize WE, Gidley DW (2003) Radiat Phys Chem 68:345
19. Dull TL, Frieze WE, Gidley DW, Sun JN, Yee AF (2001) J Phys Chem B 105:4657
20. Baklanov MR, Mogilnikov KP (2002) Microelectron Eng 64:335
21. Gibson LJ, Ashby MF (1997) Cellular solids: structure and properties, 2nd edn. Cambridge University Press, Cambridge, MA, p 186
22. Williford RE, Li XS, Addleman RS, Fryxell GE, Baskaran S, Birnbaum JC, Coyle C, Zemanian TS, Wang C, Courtney AR (2005) Micropor Mesopor Mater 85:260
23. Gross J, Fricke J (1997) J Non-Cryst Solids 95/96:1197
24. Woignier T, Reynes J, Hafidi Alaoui A, Beurroies I, Phalippou J (1999) J Non-Cryst Solids 241:45
25. Moner-Girona M, Roig A, Molins E, Martinez E, Esteve J (1999) Appl Phys Lett 75:653
26. Rodriguez-Perez MA, Alonso O, Duijsens A, Saja JA (1998) J Polym Sci, Part B: Polym Phys 36:2587
27. Gostein M, Mazurenko A, Maznev AA, Schulberg MT (2004) Micro 22(5):51
28. Vallery RS, Peng H-G, Frieze WE, Gidley DW, Moore DL, Carter RJ (2005) Res Mater Soc Symp Proc 863:B1.6.1